

Observation of $B_c^+ \rightarrow D^0 K^+$ Decays

R. Aaij *et al.*^{*}

(LHCb Collaboration)

(Received 7 January 2017; revised manuscript received 17 February 2017; published 15 March 2017)

Using proton-proton collision data corresponding to an integrated luminosity of 3.0 fb^{-1} , recorded by the LHCb detector at center-of-mass energies of 7 and 8 TeV, the $B_c^+ \rightarrow D^0 K^+$ decay is observed with a statistical significance of 5.1 standard deviations. By normalizing to $B^+ \rightarrow \bar{D}^0 \pi^+$ decays, a measurement of the branching fraction multiplied by the production rates for B_c^+ relative to B^+ mesons in the LHCb acceptance is obtained, $R_{D^0 K} = (f_c/f_u) \times \mathcal{B}(B_c^+ \rightarrow D^0 K^+) = (9.3^{+2.8}_{-2.5} \pm 0.6) \times 10^{-7}$, where the first uncertainty is statistical and the second is systematic. This decay is expected to proceed predominantly through weak annihilation and penguin amplitudes, and is the first B_c^+ decay of this nature to be observed.

DOI: 10.1103/PhysRevLett.118.111803

The B_c^+ meson is the only ground-state meson consisting of two heavy quarks of different flavor, namely a \bar{b} and a c quark. As such, its formation in pp collisions is suppressed relative to the lighter B mesons. Unlike B^0 , B^+ and B_s^0 mesons, the b -quark decay accounts for only $\sim 20\%$ of the B_c^+ width [1]. Around 70% of its width is due to c -quark decays, where the c -quark transition has been observed with $B_c^+ \rightarrow B_s^0 \pi^+$ decays [2]. This leaves $\sim 10\%$ for $\bar{b}c \rightarrow W^+ \rightarrow \bar{q}q$ annihilation amplitudes, which can be unambiguously probed in charmless final states. No charmless B_c^+ decays have been reported to date, although searches show an indication at the level of 2.4 standard deviations (σ) [3].

To test QCD factorization and explore the new physics potential of B_c^+ decays, rarer decays such as suppressed tree-level $b \rightarrow u$ transitions and $b \rightarrow s$ loop-mediated (penguin) decays can be studied, where the charm quantum number remains unchanged. The simplest decay is the color-allowed $B_c^+ \rightarrow D^{(*)0} \pi^+$ decay, illustrated in Fig. 1(a). The expected branching fraction for this decay is a factor $|V_{ub}/V_{cb}|^2 \approx 0.007$ lower than the favored $b \rightarrow c$ and color-allowed $B_c^+ \rightarrow J/\psi \pi^+$ decay [4,5], placing this mode at the limit of sensitivity with current LHCb data. However, this expectation may be enhanced by penguin and weak annihilation amplitudes, which will be more pronounced in the $B_c^+ \rightarrow D^{(*)0} K^+$ mode [see Fig. 1(b) and 1(c)]. This motivates a search for the $B_c^+ \rightarrow D^{(*)0} K^+$ and $B_c^+ \rightarrow D^{(*)0} \pi^+$ decays, particularly as the branching fraction estimates in the literature vary considerably [6–8].

*Full author list given at the end of the article.

Published by the American Physical Society under the terms of the Creative Commons Attribution 4.0 International license. Further distribution of this work must maintain attribution to the author(s) and the published article's title, journal citation, and DOI.

The decay $B^+ \rightarrow \bar{D}^0 \pi^+$ is used for normalization. Since the ratio of production rates for B_c^+ and B^+ mesons within the LHCb acceptance, f_c/f_u , is unknown, the measured observables are

$$R_{D^{(*)0} h} = \frac{f_c}{f_u} \times \mathcal{B}(B_c^+ \rightarrow D^{(*)0} h^+), \quad (1)$$

where h is π or K and $\mathcal{B}(B_c^+ \rightarrow D^{(*)0} h^+)$ represents the corresponding branching fraction. The four observables are measured with a simultaneous fit to the $D^0 \pi^+$ and $D^0 K^+$ invariant mass distributions. Theoretical estimates for $\mathcal{B}(B_c^+ \rightarrow J/\psi \pi^+)$ range from 6.0×10^{-4} [9] to 1.8×10^{-3} [10], which implies f_c/f_u values in the range 0.004–0.012 using the production ratio measured in Ref. [5] and the branching fraction $\mathcal{B}(B^+ \rightarrow J/\psi K^+)$ [11]. Estimates for $\mathcal{B}(B_c^+ \rightarrow D^0 K^+)$ vary from 1.3×10^{-7} [6] to 6.6×10^{-5} [8], while estimates for $\mathcal{B}(B_c^+ \rightarrow D^0 \pi^+)$ vary from 2.3×10^{-7} [6] to 2.3×10^{-6} [7]. Using Eq. (1), the expectation for $R_{D^0 \pi}$ is seen to cover the range $9 \times 10^{-10} - 3 \times 10^{-8}$, while $R_{D^0 K}$ covers the range $5 \times 10^{-10} - 8 \times 10^{-7}$.

This Letter reports a search for $B_c^+ \rightarrow D^0 \pi^+$ and $B_c^+ \rightarrow D^0 K^+$ decays in pp collision data corresponding to

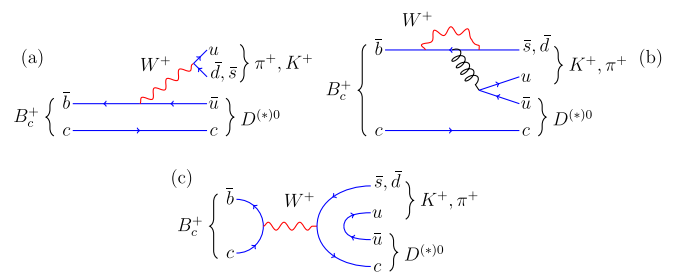


FIG. 1. Tree (a), penguin (b), and weak annihilation (c) diagrams for the decays studied. In each case, the meson appearing before the comma denotes the favored decay.

integrated luminosities of 1.0 and 2.0 fb^{-1} taken by the LHCb experiment at center-of-mass energies of 7 and 8 TeV, respectively, where the D^0 meson is reconstructed in the Cabibbo-favored final states $D^0 \rightarrow K^-\pi^+$ or $D^0 \rightarrow K^-\pi^+\pi^-\pi^+$ (inclusion of charge-conjugate processes is implied throughout). Partially reconstructed $B_c^+ \rightarrow (D^{*0} \rightarrow D^0\{\pi^0, \gamma\})h^+$ decays, where the neutral particle indicated in braces is not considered in the invariant mass calculation, are treated as additional signal channels. The number of B_c^+ decays is normalized by comparison to the number of $B^+ \rightarrow [\bar{D}^0 \rightarrow K^+\pi^-(\pi^+\pi^-)]\pi^+$ decays. A fit to the invariant mass distribution of $D^{(*)0}h^+$ candidates in the range 5800–6900 MeV/c^2 enables a measurement of

$$R_{D^{(*)0}h} = \frac{\mathcal{N}(B_c^+ \rightarrow D^{(*)0}h^+)}{\mathcal{N}(B^+ \rightarrow \bar{D}^0\pi^+)} \times \mathcal{B}(B^+ \rightarrow \bar{D}^0\pi^+) \times \xi, \quad (2)$$

where $\mathcal{N}(B_c^+ \rightarrow D^{(*)0}h^+)$ represents the $B_c^+ \rightarrow D^{(*)0}h^+$ yield, $\mathcal{N}(B^+ \rightarrow \bar{D}^0\pi^+)$ represents the yield of $B^+ \rightarrow \bar{D}^0\pi^+$ normalization decays, $\mathcal{B}(B^+ \rightarrow \bar{D}^0\pi^+)$ is the normalization mode branching fraction [11], and ξ is the ratio of efficiencies for reconstructing and selecting B^+ and B_c^+ mesons decaying to these final states.

The LHCb detector is a single-arm forward spectrometer covering the pseudorapidity range $2 < \eta < 5$, described in detail in Refs. [12,13]. The detector allows the reconstruction of both charged and neutral particles. For this analysis, the ring-imaging Cherenkov (RICH) detectors [14], distinguishing pions, kaons, and protons, are particularly important. Simulated events are produced using the software described in Refs. [15–22].

After reconstruction of the D^0 meson candidate, the same selection is applied to the B_c^+ and B^+ candidates. The invariant mass of the D^0 candidate must be within $\pm 25 \text{ MeV}/c^2$ of its known value [11]. The other hadron originating from the B decay must have transverse momentum (p_T) in the range 0.5–10.0 GeV/c and momentum (p) in the range 5–100 GeV/c , ensuring that the track is within the kinematic coverage of the RICH detectors that provide particle identification (PID) information. A kinematic fit is performed to each decay chain [23], with vertex constraints applied to both the B and D vertices, and the D^0 candidate mass constrained to its known value. The B^+ (B_c^+) meson candidates with an invariant mass in the interval 5080–5900 MeV/c^2 (5800–6900 MeV/c^2) and with a proper decay time above 0.2 ps are retained. Each B candidate is associated with the primary vertex (PV) to which it has the smallest impact parameter (IP), defined as the distance of closest approach of the candidate's trajectory to a given PV.

Two boosted decision tree (BDT) discriminators [24] are used for further background suppression. They are trained using simulated $B_c^+ \rightarrow [D^0 \rightarrow K^-\pi^+(\pi^+\pi^-)]h^+$ signal decays and a sample of wrong-sign $K^+\pi^-(\pi^+\pi^-)h^+$

combinations from data with invariant mass in the range 5900–7200 MeV/c^2 . For the first BDT, background candidates with a D^0 invariant mass more than $\pm 30 \text{ MeV}/c^2$ away from the known D^0 mass are used. In the second BDT, background candidates with a D^0 invariant mass within $\pm 25 \text{ MeV}/c^2$ of the known D^0 mass are used. A loose cut on the classifier response of the first BDT is applied before training the second one. This focuses the second BDT training on backgrounds enriched with fully reconstructed D^0 mesons.

The inputs to all BDTs include properties of each particle (p , p_T , and the IP significance) and additional properties of the B and D^0 candidates (decay time, flight distance, decay vertex quality, radial distance between the decay vertex and the PV, and the angle between the reconstructed momentum vector and the line connecting the production and decay vertices). A two-dimensional optimization is performed to determine the second stage BDT requirements for the two-body and four-body modes, where the signal S is compared to the number of background events B in data using a figure of merit $S/(\sqrt{B} + 3/2)$ [25]. The value of B is determined within $\pm 50 \text{ MeV}/c^2$ of the known B_c^+ mass. No PID information is used in the BDT training, so that the efficiency for $B \rightarrow D^0K^+$ and $B \rightarrow D^0\pi^+$ decays is similar. The use of BDTs to select signal decays was validated by comparing the efficiency of the BDT requirements for $B^+ \rightarrow \bar{D}^0\pi^+$ decays in data and simulation, where close agreement was found across a wide range of BDT cuts. The purity of the selection is further improved by requiring all kaons and pions in the D^0 decay to be identified with a PID selection that has an efficiency of about 85% per particle.

Simulated signal samples are used to evaluate the relative efficiency for selecting B_c^+ and B^+ decays. The efficiency ratio is $\xi = \epsilon(B^+)/\epsilon(B_c^+)$, where $\epsilon(B^+)$ and $\epsilon(B_c^+)$ represent the combined efficiencies of detector acceptance, trigger, reconstruction, and offline selection. As both B_c^+ and B^+ mesons are required to decay to the same final-state particles, differences between $\epsilon(B^+)$ and $\epsilon(B_c^+)$ arise due to differences in their masses and lifetimes. The B_c^+ meson lifetime is (0.507 ± 0.009) ps, which is 3.2 times shorter than that of the B^+ meson [11]. This results in a lower B_c^+ efficiency relative to B^+ by a factor 2.4, due to the proper decay time cut. The B_c^+ meson is heavier than the B^+ , which reduces by a factor 1.3 the fraction of B_c^+ decays in which all final-state particles are within the detector acceptance. However, as the BDTs are trained specifically on B_c^+ simulated decays, the offline selection efficiency is lower for B^+ decays, contributing a relative efficiency of 0.94. Overall, the efficiency ratio is $\xi = 3.04 \pm 0.16$ (2.88 ± 0.15) for the two-body (four-body) D^0 decay. The uncertainties are systematic, arising from the use of

finite simulated samples and possible mismodeling of the simulated B_c^+ lifetime and production kinematics.

To measure $\mathcal{N}(B^+ \rightarrow \bar{D}^0\pi^+)$, binned maximum likelihood fits to the invariant mass distributions of selected B^+ candidates are performed, where separate fits are employed for the two-body and four-body \bar{D}^0 modes. The total probability density function (PDF) is built from four contributions. The $B^+ \rightarrow \bar{D}^0\pi^+$ decays are modeled by the sum of two modified Gaussian functions with asymmetric power-law tails and an additional Gaussian function as used in Ref. [26], all of which share a common peak position. Misidentified $B^+ \rightarrow \bar{D}^0K^+$ candidates have an incorrect mass assignment and form a distribution displaced downward in mass, with a tail extending to lower invariant masses. They are modeled by the sum of two modified Gaussian PDFs with low-mass power-law tails. All PDF parameters are allowed to vary, with the exception of the tail parameters which are fixed to the values found in simulation.

Partially reconstructed decays form a background at invariant masses lower than that of the signal peak. This background is described by a combination of parametric PDFs, with yield and shape parameters that are allowed to vary. A linear function describes the combinatorial background. The yield of $B^+ \rightarrow \bar{D}^0K^+$ decays, where the kaon is misidentified as a pion, is fixed using a simultaneous fit to correctly identified $B^+ \rightarrow \bar{D}^0K^+$ events. Using a data-driven analysis of approximately 20 million D^{*+} decays reconstructed as $D^{*+} \rightarrow D^0\pi^+$, $D^0 \rightarrow K^-\pi^+$, the probability of kaon misidentification is determined to be 32%. The invariant mass fits to $B^+ \rightarrow (\bar{D}^0 \rightarrow K^+\pi^-)\pi^+$ and $B^+ \rightarrow (\bar{D}^0 \rightarrow K^+\pi^-\pi^+\pi^-)\pi^+$ decays determine a total observed yield $\mathcal{N}(B^+ \rightarrow \bar{D}^0\pi^+) = 309462 \pm 550$.

To measure $\mathcal{N}(B_c^+ \rightarrow D^{(*)0}h^+)$, a simultaneous invariant mass fit to the $B_c^+ \rightarrow D^0\pi^+$ and $B_c^+ \rightarrow D^0K^+$ samples is performed in the region 5800–6900 MeV/ c^2 . Two-body and four-body D -decay candidates are included, where a Gaussian PDF describes the fully reconstructed B_c^+ signals. The mean of this Gaussian is fixed to the known B_c^+ mass [11]. The width of the $B_c^+ \rightarrow D^0\pi^+$ PDF is taken from a fit to suppressed $B^+ \rightarrow (\bar{D}^0 \rightarrow \pi^+K^-)\pi^+$ decays, scaled up by a factor 1.3 to account for the difference in momenta of the decay products in $B_c^+ \rightarrow D^0\pi^+$ and $B^+ \rightarrow \bar{D}^0\pi^+$ decays. The width of the $B_c^+ \rightarrow D^0K^+$ peak is related to that of $B_c^+ \rightarrow D^0\pi^+$ decays by the ratio of the widths of the $B^+ \rightarrow \bar{D}^0K^+$ and $B^+ \rightarrow \bar{D}^0\pi^+$ peaks found in the normalization mode fits. Partially reconstructed $B_c^+ \rightarrow D^{*0}h^+$ signal decays are modeled using a combination of parametric PDFs, with yield and shape parameters that are allowed to vary. These decays contribute at lower invariant masses than the fully reconstructed signal decays, as a result of not considering the natural particle in the invariant mass calculation. An additional background component at low invariant mass is included to describe B_c^+ decays where

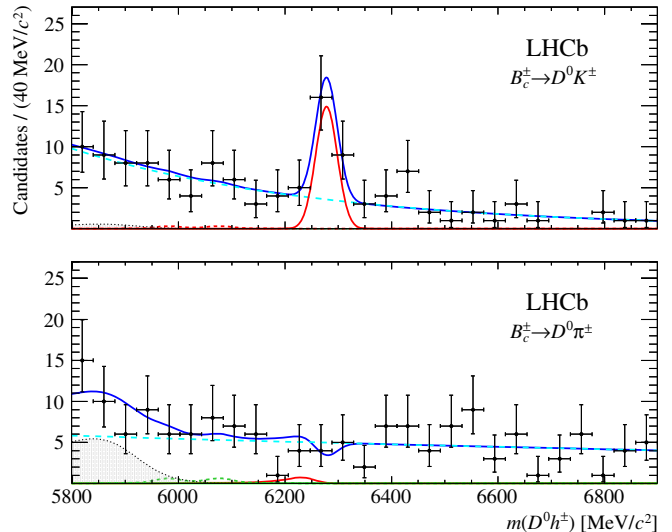


FIG. 2. Results of the simultaneous fit to the D^0K^+ (top plot) and $D^0\pi^+$ (bottom plot) invariant mass distributions in the B_c^+ mass region, including the $D^0 \rightarrow K^-\pi^+$ and $D^0 \rightarrow K^-\pi^+\pi^-\pi^+$ final states. Inclusion of the charge conjugate decays is implied. The red solid curve illustrates $B_c^+ \rightarrow D^0K^+$ decays, the red dashed curve illustrates $B_c^+ \rightarrow D^{*0}K^+$ decays, the green dashed curve represents $B_c^+ \rightarrow D^{*0}\pi^+$ decays, the gray shaded region represents partially reconstructed background decays, the cyan dashed line represents the combinatorial background, and the total PDF is displayed as a blue solid line. The small drop visible in the total $B_c^+ \rightarrow D^{(*)0}\pi^+$ PDF around the B_c^+ mass arises from the fact that the fit finds a small negative value for the $B_c^+ \rightarrow D^0\pi^+$ yield.

two particles are missed, with shape parameters taken from simulated $B^+ \rightarrow D^{*0}\pi^+\pi^0$ decays and scaled to account for the different momenta of the decay products in B_c^+ and B^+ decays.

Misidentified $B_c^+ \rightarrow D^0\pi^+(K^+)$ decays in the $B_c^+ \rightarrow D^0K^+(\pi^+)$ sample are modeled using the same PDFs as the normalization fits, with widths and peak positions scaled for the decay momentum difference. These shapes are fixed in the fit. Signal decays are split into separate samples with correct and incorrect kaon identification, with a kaon misidentification rate of 7% and a corresponding pion identification efficiency of 91% fixed using the data-driven D^{*+} analysis described above. An exponential function describes the combinatorial background, which is fitted independently in the $B_c^+ \rightarrow D^0\pi^+$ and $B_c^+ \rightarrow D^0K^+$ samples. The combinatorial yields, signal yields, and partially reconstructed $B_c^+ \rightarrow D^0h^+\{\pi^0\}$ and $B_c^+ \rightarrow D^{*0}h^+\{\pi^0\}$ background yields are all free to vary. The fit to data is shown in Fig. 2, where a $B_c^+ \rightarrow D^0K^+$ yield of 20 ± 5 events is found. All other signal yields are consistent with zero.

To test the significance of each signal yield, CL_s hypothesis tests [27] are performed. Upper limits at 95% confidence level (C.L.) are determined by the point

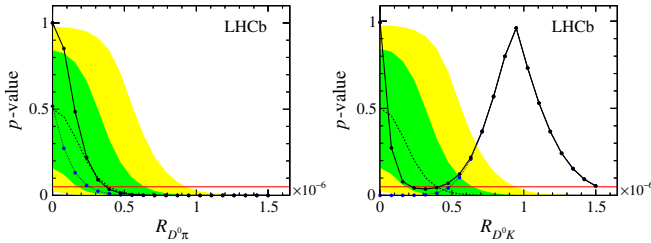


FIG. 3. CL_s p -value distributions for the R_{D^0h} observables. The dashed line represents the expected CL_s values, where the 1σ and 2σ contours are indicated by the green (dark) and yellow (light) shaded regions, respectively. Upper limits are determined by the points at which the observed CL_{s+b} p -values (black points connected by straight lines) fall below 5% (red solid line). Also displayed are the corresponding $\text{CL}_s = \text{CL}_{s+b}/\text{CL}_b$ values (blue points connected by straight dotted lines).

at which the p -value falls below 5%. All free variables in the fit are considered as nuisance parameters in this procedure. The p -value distributions for each R_{D^0h} measurement are shown in Fig. 3. The $B_c^+ \rightarrow D^{*0}h^+$ modes demonstrate no excess, and the R_{D^0h} CL_s confidence intervals are determined similarly to that of $R_{D^0\pi}$. The upper limits at 95% confidence level found for $R_{D^0\pi}$, $R_{D^{*0}\pi}$, and $R_{D^{*0}K}$ are

$$\begin{aligned} R_{D^0\pi} &< 3.9 \times 10^{-7}, \\ R_{D^{*0}\pi} &< 1.1 \times 10^{-6}, \\ R_{D^{*0}K} &< 1.1 \times 10^{-6}. \end{aligned}$$

The systematic uncertainties affecting the measurements are found to be much smaller than the statistical uncertainty, and do not alter the above upper limits.

In the case of R_{D^0K} , the observed signal is of much higher significance. To determine the full uncertainty for R_{D^0K} , the systematic uncertainties affecting the measurement are accounted for. A systematic uncertainty of 1.1×10^{-8} is incurred from the use of fixed terms in the invariant mass fit. According to Eq. (2), several terms with associated relative uncertainties scale the measured signal yield: ξ with 5.3% uncertainty, $\mathcal{B}(B^+ \rightarrow \bar{D}^0\pi^+)$ with 3.1% uncertainty [11], and $\mathcal{N}(B^+ \rightarrow \bar{D}^0\pi^+)$ with 0.14% uncertainty. The total systematic uncertainty, given by the sum in quadrature, is 6.2%.

To determine the significance of the $B_c^+ \rightarrow D^0K^+$ peak, a likelihood scan is performed. The resulting $-\Delta \log(L)$ value for the $R_{D^0K} = 0$ hypothesis corresponds to a statistical significance of $\sqrt{-2\Delta \log(L)} = 5.1\sigma$ for the signal. The final result is

$$R_{D^0K} = (9.3^{+2.8}_{-2.5}) \times 10^{-7},$$

where the first uncertainty is statistical and the second is systematic. This is the first observation of the $B_c^+ \rightarrow D^0K^+$

decay. The value of R_{D^0K} is at the high end of theoretical predictions [6–8] and an expectation based on the observed $B_c^+ \rightarrow J/\psi\pi^+$ yield at LHCb [28]. From Refs. [5] and [11], $R_{J/\psi\pi} = (7.0 \pm 0.3) \times 10^{-6}$ is obtained. As f_c/f_u is common to both $R_{J/\psi\pi}$ and R_{D^0K} , the ratio of branching fractions is measured to be $\mathcal{B}(B_c^+ \rightarrow D^0K^+)/\mathcal{B}(B_c^+ \rightarrow J/\psi\pi^+) = 0.13 \pm 0.04 \pm 0.01 \pm 0.01$, where the first uncertainty is statistical, the second is systematic, and the third comes from $R_{J/\psi\pi}$.

The absence of the $B_c^+ \rightarrow D^0\pi^+$ mode shows that the $B_c^+ \rightarrow D^0K^+$ amplitude is not dominated by the tree-level $b \rightarrow u$ transition shown in Fig. 1(a), but rather by the penguin 1(b) and/or weak annihilation 1(c) diagrams. This result constitutes the first observation of such amplitudes in the decay of a B_c^+ meson.

We express our gratitude to our colleagues in the CERN accelerator departments for the excellent performance of the LHC. We thank the technical and administrative staff at the LHCb institutes. We acknowledge support from CERN and from the national agencies: CAPES, CNPq, FAPERJ and FINEP (Brazil); NSFC (China); CNRS/IN2P3 (France); BMBF, DFG and MPG (Germany); INFN (Italy); FOM and NWO (Netherlands); MNiSW and NCN (Poland); MEN/IFA (Romania); MinES and FASO (Russia); MinECo (Spain); SNSF and SER (Switzerland); NASU (Ukraine); STFC (United Kingdom); NSF (USA). We acknowledge the computing resources that are provided by CERN, IN2P3 (France), KIT and DESY (Germany), INFN (Italy), SURF (Netherlands), PIC (Spain), GridPP (United Kingdom), RRCKI and Yandex LLC (Russia), CSCS (Switzerland), IFIN-HH (Romania), CBPF (Brazil), PL-GRID (Poland) and OSC (USA). We are indebted to the communities behind the multiple open source software packages on which we depend. Individual groups or members have received support from AvH Foundation (Germany), EPLANET, Marie Skłodowska-Curie Actions and ERC (European Union), Conseil Général de Haute-Savoie, Labex ENIGMASS and OCEVU, Région Auvergne (France), RFBR and Yandex LLC (Russia), GVA, XuntaGal and GENCAT (Spain), Herchel Smith Fund, The Royal Society, Royal Commission for the Exhibition of 1851 and the Leverhulme Trust (United Kingdom).

-
- [1] I. P. Gouz, V. V. Kiselev, A. K. Likhoded, V. I. Romanovsky, and O. P. Yushchenko, Prospects for the B_c studies at LHCb, *Phys. At. Nucl.* **67**, 1559 (2004).
 - [2] R. Aaij *et al.* (LHCb Collaboration), Observation of the Decay $B_c^+ \rightarrow B_s^0\pi^+$, *Phys. Rev. Lett.* **111**, 181801 (2013).
 - [3] R. Aaij *et al.* (LHCb Collaboration), Study of B_c^+ decays to the $K^+K^-\pi^+$ final state and evidence for the decay $B_c^+ \rightarrow \chi_{c0}\pi^+$, *Phys. Rev. D* **94**, 091102 (2016).

- [4] V. M. Abazov *et al.* (D0 Collaboration), Observation of the B_c Meson in the Exclusive Decay $B_c \rightarrow J/\psi\pi$, Phys. Rev. Lett. **101**, 012001 (2008).
- [5] R. Aaij *et al.* (LHCb Collaboration), Measurement of B_c^+ Production at $\sqrt{s} = 8$ TeV, Phys. Rev. Lett. **114**, 132001 (2015).
- [6] H. F. Fu, Y. Jiang, C. S. Kim, and G.-L. Wang, Probing non-leptonic two-body decays of B_c meson, J. High Energy Phys. **06** (2011) 15.
- [7] D.-S. Du and Z.-T. Wei, Space-like Penguin effects in B_c decays, Eur. Phys. J. C **5**, 705 (1998).
- [8] J. Zhang and X.-Q. Yu, Branching ratio and CP violation of $B_c \rightarrow DK$ decays in the perturbative QCD approach, Eur. Phys. J. C **63**, 435 (2009).
- [9] D. Ebert, R. N. Faustov, and V. O. Galkin, Weak decays of the B_c meson to charmonium and D mesons in the relativistic quark model, Phys. Rev. D **68**, 094020 (2003).
- [10] C.-H. Chang and Y.-Q. Chen, Decays of the B_c meson, Phys. Rev. D **49**, 3399 (1994).
- [11] C. Patrignani *et al.* (Particle Data Group Collaboration), Review of particle physics, Chin. Phys. C **40**, 100001 (2016).
- [12] A. A. Alves Jr. *et al.* (LHCb Collaboration), The LHCb detector at the LHC, J. Instrum. **3**, S08005 (2008).
- [13] R. Aaij *et al.* (LHCb Collaboration), LHCb detector performance, Int. J. Mod. Phys. A **30**, 1530022 (2015).
- [14] M. Adinolfi *et al.*, Performance of the LHCb RICH detector at the LHC, Eur. Phys. J. C **73**, 2431 (2013).
- [15] T. Sjöstrand, S. Mrenna, and P. Skands, PYTHIA 6.4 physics and manual, J. High Energy Phys. **05** (2006) 026.
- [16] T. Sjöstrand, S. Mrenna, and P. Skands, A brief introduction to PYTHIA 8.1, Comput. Phys. Commun. **178**, 852 (2008).
- [17] I. Belyaev *et al.*, Handling of the generation of primary events in Gauss, the LHCb simulation framework, J. Phys. Conf. Ser. **331**, 032047 (2011).
- [18] D. J. Lange, The EvtGen particle decay simulation package, Nucl. Instrum. Methods Phys. Res., Sect. A **462**, 152 (2001).
- [19] J. Allison *et al.* (Geant4 Collaboration), Geant4 developments and applications, IEEE Trans. Nucl. Sci. **53**, 270 (2006).
- [20] S. Agostinelli *et al.* (Geant4 Collaboration), Geant4: A simulation toolkit, Nucl. Instrum. Methods Phys. Res., Sect. A **506**, 250 (2003).
- [21] M. Clemencic, G. Corti, S. Easo, C. R. Jones, S. Miglioranza, M. Pappagallo, and P. Robbe, The LHCb simulation application, Gauss: Design, evolution and experience, J. Phys. Conf. Ser. **331**, 032023 (2011).
- [22] C.-H. Chang, C. Driouichi, P. Eerola, and X.-G. Wu, BCVEGPY: An event generator for hadronic production of the B_c meson, Comput. Phys. Commun. **159**, 192 (2004).
- [23] W. D. Hulsbergen, Decay chain fitting with a Kalman filter, Nucl. Instrum. Methods Phys. Res., Sect. A **552**, 566 (2005).
- [24] B. P. Roe, H.-J. Yang, J. Zhu, Y. Liu, I. Stancu, and G. McGregor, Boosted decision trees as an alternative to artificial neural networks for particle identification, Nucl. Instrum. Methods Phys. Res., Sect. A **543**, 577 (2005).
- [25] G. Punzi, in *Statistical Problems in Particle Physics, Astrophysics, and Cosmology*, edited by L. Lyons, R. Mount, and R. Reitmeyer (Stanford Linear Accelerator Center, Stanford, California, 2003), p. 79.
- [26] R. Aaij *et al.* (LHCb Collaboration), Measurement of CP observables in $B^\pm \rightarrow DK^\pm$ and $B^\pm \rightarrow D\pi^\pm$ with two- and four-body D meson decays, Phys. Lett. B **760**, 117 (2016).
- [27] L. Moneta *et al.*, The RooStats Project, Proc. Sci., ACAT20102010 (2010) 057.
- [28] R. Aaij *et al.* (LHCb Collaboration), Measurement of the branching fraction ratio $\mathcal{B}(B_c^+ \rightarrow \psi(2S)\pi^+)/\mathcal{B}(B_c^+ \rightarrow J/\psi\pi^+)$, Phys. Rev. D **92**, 072007 (2015).

R. Aaij,⁴⁰ B. Adeva,³⁹ M. Adinolfi,⁴⁸ Z. Ajaltouni,⁵ S. Akar,⁵⁹ J. Albrecht,¹⁰ F. Alessio,⁴⁰ M. Alexander,⁵³ S. Ali,⁴³ G. Alkhazov,³¹ P. Alvarez Cartelle,⁵⁵ A. A. Alves Jr.,⁵⁹ S. Amato,² S. Amerio,²³ Y. Amhis,⁷ L. An,³ L. Anderlini,¹⁸ G. Andreassi,⁴¹ M. Andreotti,^{17,g} J. E. Andrews,⁶⁰ R. B. Appleby,⁵⁶ F. Archilli,⁴³ P. d'Argent,¹² J. Arnaud Romeu,⁶ A. Artamonov,³⁷ M. Artuso,⁶¹ E. Aslanides,⁶ G. Auriemma,²⁶ M. Baalouch,⁵ I. Babuschkin,⁵⁶ S. Bachmann,¹² J. J. Back,⁵⁰ A. Badalov,³⁸ C. Baesso,⁶² S. Baker,⁵⁵ V. Balagura,^{7,c} W. Baldini,¹⁷ R. J. Barlow,⁵⁶ C. Barschel,⁴⁰ S. Barsuk,⁷ W. Barter,⁵⁶ F. Baryshnikov,³² M. Baszczyk,²⁷ V. Batozskaya,²⁹ B. Batsukh,⁶¹ V. Battista,⁴¹ A. Bay,⁴¹ L. Beauchourt,⁴ J. Beddow,⁵³ F. Bedeschi,²⁴ I. Bediaga,¹ L. J. Bel,⁴³ V. Bellee,⁴¹ N. Belloli,^{21,i} K. Belous,³⁷ I. Belyaev,³² E. Ben-Haim,⁸ G. Bencivenni,¹⁹ S. Benson,⁴³ A. Berezhnoy,³³ R. Bernet,⁴² A. Bertolin,²³ C. Betancourt,⁴² F. Betti,¹⁵ M.-O. Bettler,⁴⁰ M. van Beuzekom,⁴³ Ia. Bezshyiko,⁴² S. Bifani,⁴⁷ P. Billoir,⁸ T. Bird,⁵⁶ A. Birnkraut,¹⁰ A. Bitadze,⁵⁶ A. Bizzeti,^{18,u} T. Blake,⁵⁰ F. Blanc,⁴¹ J. Blouw,^{11,f} S. Blusk,⁶¹ V. Bocci,²⁶ T. Boettcher,⁵⁸ A. Bondar,^{36,w} N. Bondar,^{31,40} W. Bonivento,¹⁶ I. Bordyuzhin,³² A. Borgheresi,^{21,i} S. Borghi,⁵⁶ M. Borisjak,³⁵ M. Borsato,³⁹ F. Bossu,⁷ M. Bouabdil,⁹ T. J. V. Bowcock,⁵⁴ E. Bowen,⁴² C. Bozzi,^{17,40} S. Braun,¹² M. Britsch,¹² T. Britton,⁶¹ J. Brodzicka,⁵⁶ E. Buchanan,⁴⁸ C. Burr,⁵⁶ A. Bursche,² J. Buytaert,⁴⁰ S. Cadeddu,¹⁶ R. Calabrese,^{17,g} M. Calvi,^{21,i} M. Calvo Gomez,^{38,m} A. Camboni,³⁸ P. Campana,¹⁹ D. H. Campora Perez,⁴⁰ L. Capriotti,⁵⁶ A. Carbone,^{15,e} G. Carboni,^{25,j} R. Cardinale,^{20,h} A. Cardini,¹⁶ P. Carniti,^{21,i} L. Carson,⁵² K. Carvalho Akiba,² G. Casse,⁵⁴ L. Cassina,^{21,i} L. Castillo Garcia,⁴¹ M. Cattaneo,⁴⁰ G. Cavallero,²⁰ R. Cenci,^{24,t} D. Chamont,⁷ M. Charles,⁸ Ph. Charpentier,⁴⁰ G. Chatzikonstantinidis,⁴⁷ M. Chefdeville,⁴ S. Chen,⁵⁶ S. -F. Cheung,⁵⁷ V. Chobanova,³⁹

- ¹⁷Sezione INFN di Ferrara, Ferrara, Italy
¹⁸Sezione INFN di Firenze, Firenze, Italy
¹⁹Laboratori Nazionali dell'INFN di Frascati, Frascati, Italy
²⁰Sezione INFN di Genova, Genova, Italy
²¹Sezione INFN di Milano Bicocca, Milano, Italy
²²Sezione INFN di Milano, Milano, Italy
²³Sezione INFN di Padova, Padova, Italy
²⁴Sezione INFN di Pisa, Pisa, Italy
²⁵Sezione INFN di Roma Tor Vergata, Roma, Italy
²⁶Sezione INFN di Roma La Sapienza, Roma, Italy
²⁷Henryk Niewodniczanski Institute of Nuclear Physics Polish Academy of Sciences, Kraków, Poland
²⁸AGH - University of Science and Technology, Faculty of Physics and Applied Computer Science, Kraków, Poland
²⁹National Center for Nuclear Research (NCBJ), Warsaw, Poland
³⁰Horia Hulubei National Institute of Physics and Nuclear Engineering, Bucharest-Magurele, Romania
³¹Petersburg Nuclear Physics Institute (PNPI), Gatchina, Russia
³²Institute of Theoretical and Experimental Physics (ITEP), Moscow, Russia
³³Institute of Nuclear Physics, Moscow State University (SINP MSU), Moscow, Russia
³⁴Institute for Nuclear Research of the Russian Academy of Sciences (INR RAN), Moscow, Russia
³⁵Yandex School of Data Analysis, Moscow, Russia
³⁶Budker Institute of Nuclear Physics (SB RAS), Novosibirsk, Russia
³⁷Institute for High Energy Physics (IHEP), Protvino, Russia
³⁸ICCUB, Universitat de Barcelona, Barcelona, Spain
³⁹Universidad de Santiago de Compostela, Santiago de Compostela, Spain
⁴⁰European Organization for Nuclear Research (CERN), Geneva, Switzerland
⁴¹Institute of Physics, Ecole Polytechnique Fédérale de Lausanne (EPFL), Lausanne, Switzerland
⁴²Physik-Institut, Universität Zürich, Zürich, Switzerland
⁴³Nikhef National Institute for Subatomic Physics, Amsterdam, Netherlands
⁴⁴Nikhef National Institute for Subatomic Physics and VU University Amsterdam, Amsterdam, Netherlands
⁴⁵NSC Kharkiv Institute of Physics and Technology (NSC KIPT), Kharkiv, Ukraine
⁴⁶Institute for Nuclear Research of the National Academy of Sciences (KINR), Kyiv, Ukraine
⁴⁷University of Birmingham, Birmingham, United Kingdom
⁴⁸H.H. Wills Physics Laboratory, University of Bristol, Bristol, United Kingdom
⁴⁹Cavendish Laboratory, University of Cambridge, Cambridge, United Kingdom
⁵⁰Department of Physics, University of Warwick, Coventry, United Kingdom
⁵¹STFC Rutherford Appleton Laboratory, Didcot, United Kingdom
⁵²School of Physics and Astronomy, University of Edinburgh, Edinburgh, United Kingdom
⁵³School of Physics and Astronomy, University of Glasgow, Glasgow, United Kingdom
⁵⁴Oliver Lodge Laboratory, University of Liverpool, Liverpool, United Kingdom
⁵⁵Imperial College London, London, United Kingdom
⁵⁶School of Physics and Astronomy, University of Manchester, Manchester, United Kingdom
⁵⁷Department of Physics, University of Oxford, Oxford, United Kingdom
⁵⁸Massachusetts Institute of Technology, Cambridge, Massachusetts, USA
⁵⁹University of Cincinnati, Cincinnati, Ohio, USA
⁶⁰University of Maryland, College Park, Maryland, USA
⁶¹Syracuse University, Syracuse, New York, USA
⁶²Pontifícia Universidade Católica do Rio de Janeiro (PUC-Rio), Rio de Janeiro, Brazil,
associated with Universidade Federal do Rio de Janeiro (UFRJ), Rio de Janeiro, Brazil
⁶³University of Chinese Academy of Sciences, Beijing, China,
associated with Center for High Energy Physics, Tsinghua University, Beijing, China
⁶⁴School of Physics and Technology, Wuhan University, Wuhan, China,
associated with Center for High Energy Physics, Tsinghua University, Beijing, China
⁶⁵Institute of Particle Physics, Central China Normal University, Wuhan, Hubei, China,
associated with Center for High Energy Physics, Tsinghua University, Beijing, China
⁶⁶Departamento de Física, Universidad Nacional de Colombia, Bogota, Colombia,
associated with LPNHE, Université Pierre et Marie Curie, Université Paris Diderot, CNRS/IN2P3, Paris, France
⁶⁷Institut für Physik, Universität Rostock, Rostock, Germany,
associated with Physikalisch-Technische Bundesanstalt, Braunschweig, Germany
⁶⁸National Research Centre Kurchatov Institute, Moscow, Russia,
associated with Institute of Theoretical and Experimental Physics (ITEP), Moscow, Russia

⁶⁹*Instituto de Fisica Corpuscular, Centro Mixto Universidad de Valencia - CSIC, Valencia, Spain,*

associated with ICCUB, Universitat de Barcelona, Barcelona, Spain

⁷⁰*Van Swinderen Institute, University of Groningen, Groningen, Netherlands,*

*associated with Nikhef National Institute for Subatomic Physics,
Amsterdam, Netherlands*

[†]Deceased.

^aUniversidade Federal do Triângulo Mineiro (UFTM), Uberaba-MG, Brazil.

^bLaboratoire Leprince-Ringuet, Palaiseau, France.

^cP.N. Lebedev Physical Institute, Russian Academy of Science (LPI RAS), Moscow, Russia.

^dUniversità di Bari, Bari, Italy.

^eUniversità di Bologna, Bologna, Italy.

^fUniversità di Cagliari, Cagliari, Italy.

^gUniversità di Ferrara, Ferrara, Italy.

^hUniversità di Genova, Genova, Italy.

ⁱUniversità di Milano Bicocca, Milano, Italy.

^jUniversità di Roma Tor Vergata, Roma, Italy.

^kUniversità di Roma La Sapienza, Roma, Italy.

^lAGH - University of Science and Technology, Faculty of Computer Science, Electronics and Telecommunications, Kraków, Poland.

^mLIFAELS, La Salle, Universitat Ramon Llull, Barcelona, Spain.

ⁿHanoi University of Science, Hanoi, Viet Nam.

^oUniversità di Padova, Padova, Italy.

^pUniversità di Pisa, Pisa, Italy.

^qUniversità degli Studi di Milano, Milano, Italy.

^rUniversità di Urbino, Urbino, Italy.

^sUniversità della Basilicata, Potenza, Italy.

^tScuola Normale Superiore, Pisa, Italy.

^uUniversità di Modena e Reggio Emilia, Modena, Italy.

^vIligan Institute of Technology (IIT), Iligan, Philippines.

^wNovosibirsk State University, Novosibirsk, Russia.